nature electronics

Article

https://doi.org/10.1038/s41928-023-00995-z

# Optically and radiofrequency-transparent metadevices based on quasi-one-dimensional surface plasmon polariton structures

Received: 4 August 2022

Accepted: 14 June 2023

Published online: 13 July 2023

Check for updates

Hao-Ran Zu[1], Bian Wu[1] ✉, Biao Chen[1], Wen-Hua Li[1], Tao Su[1], Ying Liu[1], Wen-Xuan Tang[2], Da-Ping He[3] & Tie-Jun Cui[2] ✉

Transparent metadevices could equip electronic systems with unique functionalities such as anti-interference and stealth capabilities. However, optically transparent devices currently rely on transparent conductive materials, which have low optical transmittance, low operating efficiency and an inability to achieve radiofrequency transparency. Here, we show that metadevices based on quasi-one-dimensional surface plasmon polariton structures can offer optical and radiofrequency transparency. The structures are composed of subwavelength unit cells created from fine metallic lines printed on a flexible and transparent substrate. The approach can be used to create arbitrarily shaped waveguides with topological robustness for transmission applications, and converters for changing surface plasmon polariton waves into space waves for radiation applications. To illustrate the potential of the technology, we use the microwave metadevices to construct a wireless communication scheme for image transfer.

Transparent electronics are of potential use in applications such as optical and electromagnetic stealth, solar energy technology and integrated communications[1–10]. However, optically transparent electronics typically rely on the properties of conductive materials such as indium tin oxide (ITO)[6–8]. These methods are limited by the intrinsic characteristics of the materials. First, the conductivity (carrier density) and optical transparency are mutually restricted[7,8], which reduces the optical transmittance or the performance of the device. In communication systems, for example, ITO can only be applied to miniature devices due to the balance between optical transparency and device performance, and the operating efficiency often suffers from deterioration[11,12]. Second, these optically transparent conductor materials are not radiofrequency transparent, which means that the devices are of limited use in electromagnetic stealth and integrated communications.

Metamaterials can be designed to have unique electromagnetic properties[13–17]. Such periodic structures[18–22] can be used to control surface plasmon polaritons (SPPs), creating applications in biomedical sensing[23], near-field microscopy[24], laser technology[25–27], low-crosstalk transmission[28], frequency-domain filtering[29] and integrated communications[30,31]. SPP structures can also be used to concentrate, channel and enhance energy[32–37], extending the potential application of such systems. However, the use of SPPs in the development of optical and radiofrequency transparency remains limited.

In this Article, we show that metadevices with optical and radiofrequency transparency can be created using quasi-one-dimensional (quasi-1D) SPP structures. The quasi-1D structures, which are composed of fine metallic lines, can provide confined SPP waves, while offering 90.8% optical transmittance and 96.5% radiofrequency transmittance. The approach can be used to create arbitrarily shaped quasi-1D SPP waveguides, and we create 'SPP'-shaped waveguides, as well as converters for turning SPP waves into space waves. We also developed a wireless communication scheme for

[1]National Key Laboratory of Antennas and Microwave Technology, Xidian University, Xi'an, China. [2]State Key Laboratory of Millimeter Waves, Southeast University, Nanjing, China. [3]Hubei Engineering Research Center of RF–Microwave Technology and Application, Wuhan University of Technology, Wuhan, China. ✉e-mail: bwu@mail.xidian.edu.cn; tjcui@seu.edu.cn

image transfer, using the quasi-1D SPP metadevices to transmit and radiate signals.

## Transparent quasi-1D structured SPPs

Our quasi-1D structured SPPs are composed of subwavelength unit cells created from fine metallic lines printed on a polyethylene terephthalate (PET) substrate (Fig. 1a). The SPP mode can be effectively confined and channelled by the metallic lines, while offering excellent transmittances for both optical and radiofrequency incidences.

High confinement is a key feature of SPPs, and can provide field enhancement and subwavelength resolution. To ensure that the quasi-1D structured SPPs can achieve optical and radiofrequency transparency without sacrificing high confinement, it is necessary to first evaluate the performance of field confinement. Figure 1b–d depicts the energy confinement comparison of three-dimensional (3D), two-dimensional (2D) and quasi-1D structured SPPs; the perfect-conductor structures, which are calculated with the finite-integration technique using CST Microwave Studio, are adopted. The geometric parameters of the three SPP structures are all the same (as given in Fig. 2a) apart from the thicknesses of 5 mm, 1 μm and 1 μm for the 3D, 2D and quasi-1D structures respectively, and the linewidth of the quasi-1D structures is 100 μm.

The quasi-1D structures are found to confine the SPP mode to a smaller region than do the other structures, providing higher spatial confinement while maintaining similar distributions of electric currents. The elaborate topology of the quasi-1D SPP structure retains the edge of the traditional SPP structure, which guides the electric current and is important for maintaining the current distribution and supporting the SPP mode.

Higher energy confinement usually contributes to lower plasma frequency and greater field enhancement of SPPs. Figure 1e plots the dispersion relations of the three kinds of SPP structure. The dispersion curves of the 3D and 2D SPP structures are almost the same, which indicates similar plasma frequencies and wavelengths. In comparison, the quasi-1D structures achieve lower plasma frequency and shortened wavelength at the same frequency (Supplementary Note 1). Figure 1f,g shows the electric field distributions along two directions of the cross-sections (the white dotted lines in Fig. 1b–d). The field amplitudes decay exponentially along the two orthogonally lateral (*Y* and *Z*) directions, illustrating the typical features of SPP modes. It is observed that the quasi-1D SPP structures offer immensely increased field enhancement when compared with the 2D and 3D structures, benefiting from the higher confinement. These results indicate that the quasi-1D SPP structures for achieving optical and radiofrequency transparency can support highly confined SPP modes well, even offering higher confinement with shorter wavelength and greater field enhancement. Further, the higher field confinement brought by the quasi-1D SPP structures can benefit microwave devices in achieving miniaturization, realizing integration and suppressing signal crosstalk (Supplementary Note 2).

To describe the characteristics and the controllable designs of quasi-1D structured SPPs in detail, we demonstrate the manipulations of the dispersion relation, wavelength and field enhancement with the goal of achieving on-demand tailored SPPs. The designed SPP unit cell is depicted in Fig. 2a, and consists of the quasi-1D metallic structure and the PET substrate with a thickness of $t_2$. The quasi-1D metal structure has a pectinate shape with period $p$, groove depth $h$ and groove width $a$, and the metal lines have a thickness of $t_1$ and width of $w$. For comprehensive analyses, the actual electrical conductivity of copper is adopted, and a PET substrate with a dielectric constant of 3.3 and a loss tangent of 0.003 is considered. The quasi-1D structures can also support the SPP mode with ultrafine metal lines (Supplementary Note 3); the width of these metal lines is set to 5 μm, which is negligible for the operating wavelength.

Figure 2b shows the variation of the dispersion relation with different $h$ of the SPP unit cell. The dispersion curves deviate from the light line, indicating that the SPPs possess larger wave vector and shorter wavelength. As $h$ ranges from 1 mm to 3 mm, the plasma frequency significantly decreases, which usually leads to shorter wavelength, higher confinement and lower operating band[38] (Supplementary Note 4). In this way, the dispersion relation, as well as the plasma frequencies and wavelengths at specific frequencies, can be controlled by the geometric parameters of the quasi-1D structure. For instance, at 8 GHz, $\lambda_1$ ($h$ = 1 mm) > $\lambda_2$ ($h$ = 2 mm) > $\lambda_3$ ($h$ = 3 mm) is calculated in Fig. 2b. Correspondingly, Fig. 2c shows the electric field distributions at 8 GHz in the planes 2 mm above three quasi-1D SPP structures with the same length but different $h$. It is obvious that different SPP wavelengths are achieved with different $h$, which is consistent with Fig. 2b. Moreover, Fig. 2d,e plots the electric field amplitudes along the *Y* direction and *Z* direction with different $h$ at 8 GHz. With increasing $h$, the field enhancement and confinement can be controlled. Furthermore, the manipulation for transmission efficiency of the quasi-1D structured SPPs is also qualified by adjusting the metal linewidth (Supplementary Note 5). This analysis indicates that tailored SPPs can be achieved by manipulation of the quasi-1D SPP structures.

## Optically and radiofrequency-transparent metadevices

To demonstrate the potential of the quasi-1D structured SPPs in optically and radiofrequency-transparent metadevices, we fabricated some prototypes to verify the optical and radiofrequency transmittance of the quasi-1D SPP structures, and demonstrated transmission-type and radiation-type metadevices.

Figure 3a shows photographs and scanning electron microscopy images of the quasi-1D SPP structures with different $h$, corresponding to Fig. 1a. With a copper linewidth of 5 μm, the quasi-1D SPP structures are fabricated on a 100-μm-thickness PET substrate, showing great flexibility and excellently optical transparency (Supplementary Video 1 sample 1). These quasi-1D SPP unit cells periodically arranged along the *X* direction constitute the SPP waveguides (Supplementary Video 1 sample 2), which can support the planar and conformal transmission of SPP modes (Supplementary Note 6).

To analyse the optical and radiofrequency transparency of the SPPs structures, we cover the entire 2D plane periodically with the SPP unit cells, forming a periodic unit cell array. Here, the quasi-1D structured SPP unit cell with $h$ = 1 mm is selected for the periodic arrangement, in which other geometric parameters are the same as those in Fig. 2a. Figure 3b shows the schematic diagram of the periodic SPP unit-cell array, and the transmittances in the optical and radiofrequency bands can be evaluated. For the optical band, the area percentage of opaque materials can be used to evaluate the optical transmittance and optical reflectance of structures whose dimension is much larger than the optical wavelength[39]. For the radiofrequency band, the transmittance and reflectance are calculated with finite-element analysis using CST Microwave Studio.

Optical and radiofrequency transmittances are closely related to the metal linewidth of the quasi-1D structures, and smaller linewidth tends to bring higher transmittances. For a fixed metal linewidth, the transmittance increases as the frequency increases in the radiofrequency band. We also provide specific analyses for the optical band and radiofrequency band with different polarizations (Supplementary Note 7).

The SPP unit-cell array shows good transparency and flexibility (Supplementary Video 1 sample 3). Figure 3c plots the optical transmittances of the PET substrate and the SPP unit-cell array, measured using a Hitachi UH4150 spectrometer. Over the visible spectrum (380–780 nm), the experimental optical transmittance is above 90%, which is little different from the transmittance of the PET substrate. Moreover, we measured the radiofrequency transmittance in an anechoic chamber (Supplementary Note 8) and the experimental results are shown in Fig. 3d. Over the typical band (18–40 GHz, covering the

https://doi.org/10.1038/s41928-023-00995-z

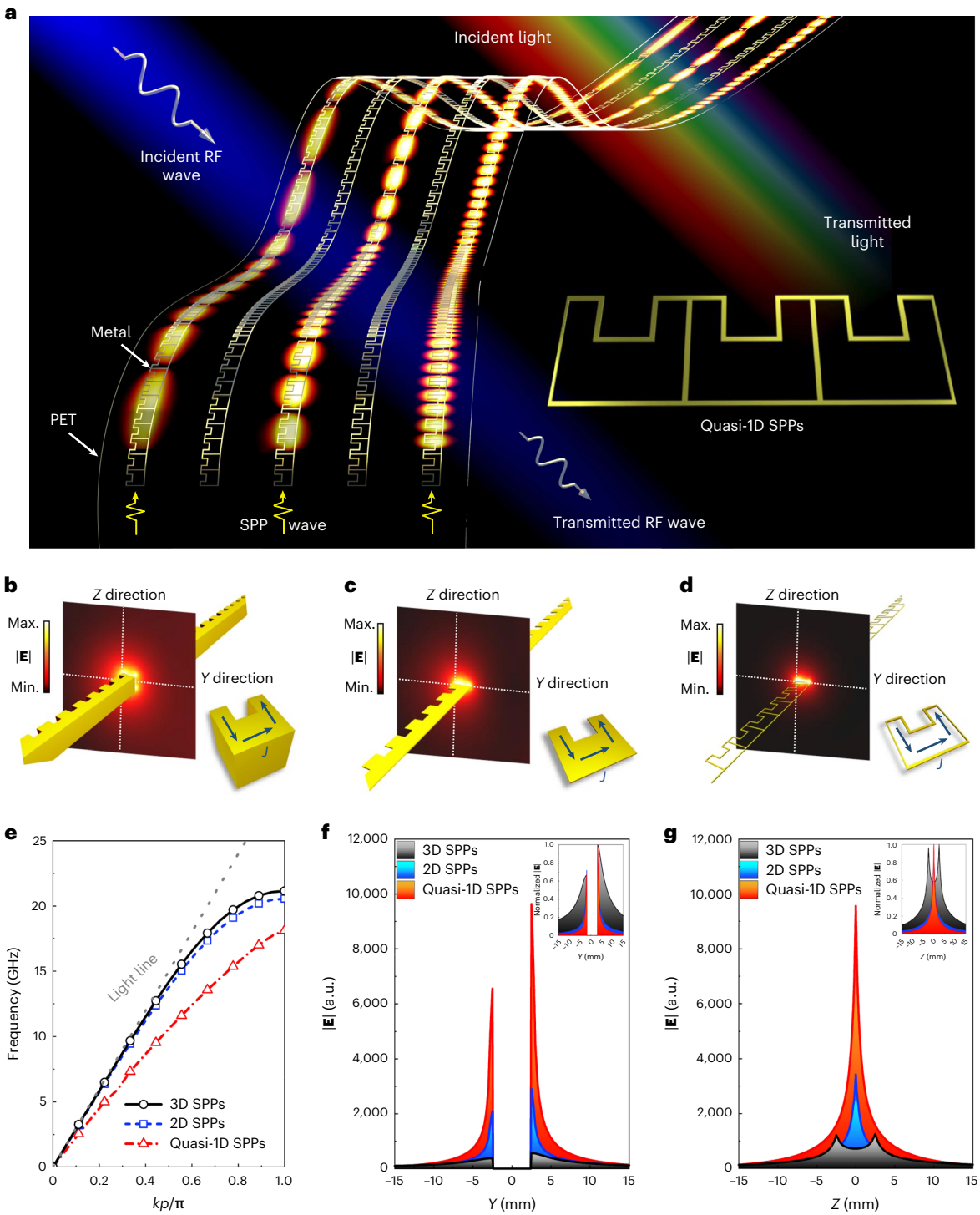


**Fig. 1 | Configuration and characteristics of the quasi-1D structured SPPs.** **a**, Schematic of the quasi-1D structured SPPs. RF, radiofrequency. **b**–**d**, Energy confinement comparison of 3D, 2D and quasi-1D structured SPPs. *J*, electric current; the quasi-1D structures achieve higher confinement. **e**, Dispersion relations of 3D, 2D and quasi-1D structured SPPs. *k*, wavenumber. *p*, period of quasi-1D SPP structures; the quasi-1D structures exhibit lower plasma frequency and shorter wavelength. **f**,**g**, Electric field amplitudes |**E**| along *Y* direction (**f**) and *Z* direction (**g**) of the 3D, 2D and quasi-1D structures; the quasi-1D structures show greater field enhancement and higher confinement. a.u., arbitrary units.

commonly used K/$K_a$ bands of radar detection and 5G millimetre communication bands), the experimental radiofrequency transmittance is still above 90%. The average transmittances within the visible spectrum and the radiofrequency band reach 90.8% and 96.5% respectively, exhibiting excellent optical and radiofrequency transparency simultaneously.

Since the quasi-1D structured SPPs possess high confinement, the energy can be concentrated and channelled along the structures, showing excellent topological robustness for realizing arbitrary-shape SPP waveguides. Figure 4a shows photographs of SPP-shaped quasi-1D SPP waveguides, which exhibit excellent transparency and are nearly invisible. The shape of the letters SPP is formed by arranging the quasi-1D

https://doi.org/10.1038/s41928-023-00995-z

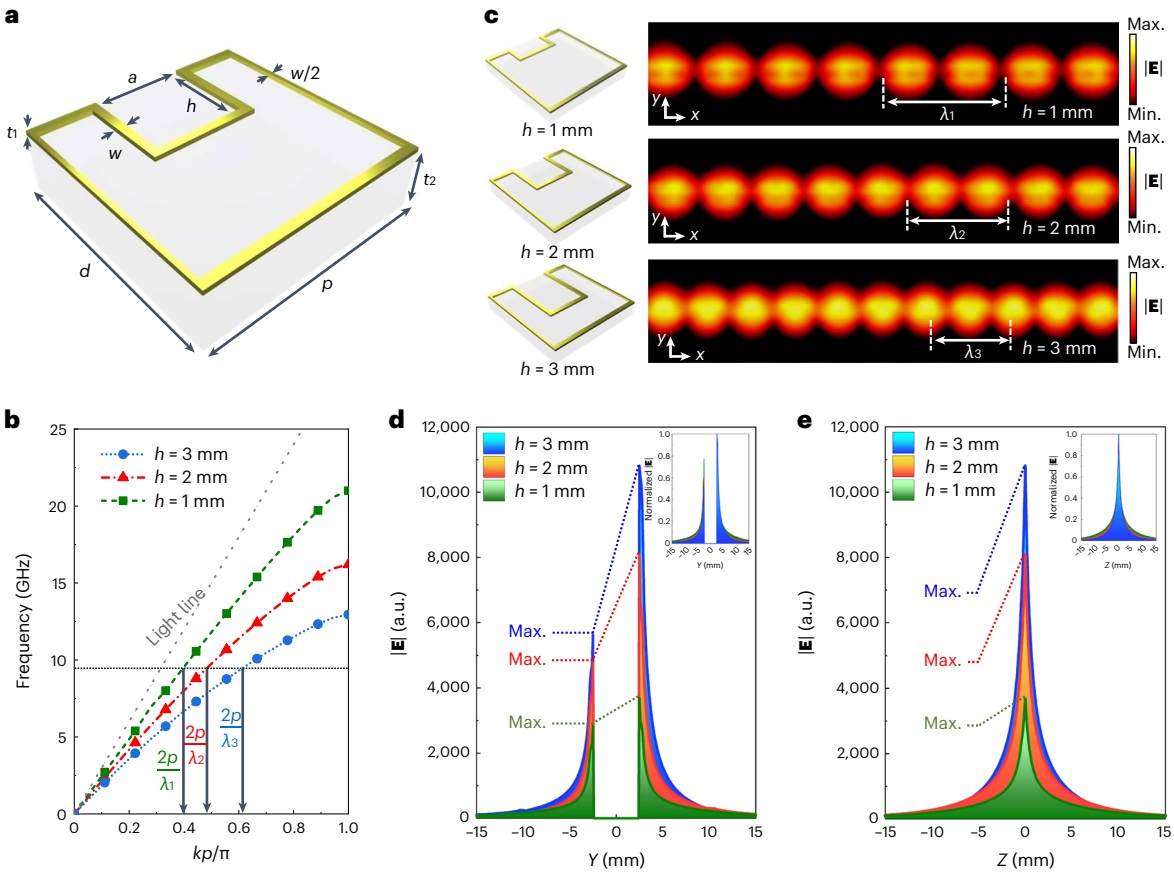


**Fig. 2 | Manipulation of the quasi-1D structured SPPs. a**, Geometric parameters of the designed SPP unit cell, with $a = 2$ mm, $h = 2$ mm, $d = 5$ mm, $p = 5$ mm, $t_1 = 1$ μm, $w = 5$ μm and $t_2 = 100$ μm. **b**, Variation of the designed SPP unit-cell dispersion relation with different values of $h$; controllable dispersion is provided. **c** Electric field distributions at 2 mm above the quasi-1D SPP structures over the same length with different $h$ at 8 GHz; controllable wavelength can be observed. **d**,**e**, Electric field amplitudes along $Y$ direction (**d**) and $Z$ direction (**e**) of quasi-1D SPP structures with different $h$ at 8 GHz; controllable enhancement and confinement are realized.

structured SPP unit cells. As depicted in Fig. 4b,c, the characters SPP are portrayed with highly enhanced and confined electric fields at 8 GHz, showing excellent topological robustness with low radiation loss (Supplementary Note 9).

Energy confinement can be manipulated in the quasi-1D structured SPPs by adjusting the geometrical parameters. Hence, we fabricated an SPP wave to space wave converter. By gradually reducing the groove depth of the quasi-1D structures, the energy confinement of the structures is gradually weakened, and the matching from the strongly confined SPP waves to the weakly confined space waves is finally completed. Figure 4d shows a photograph of the quasi-1D structured SPP wave to space wave converter: the configuration is nearly invisible. Figure 4e,f shows the calculated and experimental electric field distributions of the converter at 10 GHz. It is observed that the groove depth in the first half of the converter is constant to support strongly confined SPP waves, and the groove depth in the second half decreases linearly to zero. In this way, confinement of the SPP mode gradually decreases, and finally the SPP waves are transformed completely into space waves to form stable endfire radiation.

## Optically and radiofrequency-transparent wireless communication scheme

In complex electromagnetic environments, where various electronic devices coexist, the demand for integrated communication, optical stealth and electromagnetic stealth is increasing. Many scenarios (such as solar energy harvesting, urban densification communication and vehicle-mounted communication) seek a wireless communication system that can provide high signal strength and excellent optical and radiofrequency transmittance. Such a communication system should be easily integrated into various transparent objects (such as windows of office buildings, vehicle-mounted glass, digital screens, solar panels) without deteriorating the communication and energy collection of the original electronic devices. Our optically and radiofrequency-transparent metadevices could provide such capabilities.

To validate the approach, a realistic wireless communication system was built to perform direct data transmission. Figure 5 shows a schematic of our approach to optically and radiofrequency-transparent metadevice-based wireless communication. In this scheme, the image (the logo of Xidian University) with a 534 pt × 490 pt pixel is directly transmitted under a carrier frequency of 5.8 GHz: the computer digitizes the image, the signal processing module converts the data into the radiofrequency signal, and then the radiofrequency signal is fed into the transceiver. The transceiver is composed of the coplanar waveguide, quasi-1D SPP waveguides and quasi-1D SPP antennas, which respectively realize signal feeding, signal transmission and signal radiation to complete wireless communication. To illustrate the capabilities of the wireless communication scheme, and provide a comparison with a traditional ITO-based approach, the experiments were divided into two categories: a quasi-1D SPP-based/ITO-based data transfer without a barrier; and quasi-1D SPP-based data transfer with a quasi-1D SPP-based/ITO-based barrier.

https://doi.org/10.1038/s41928-023-00995-z

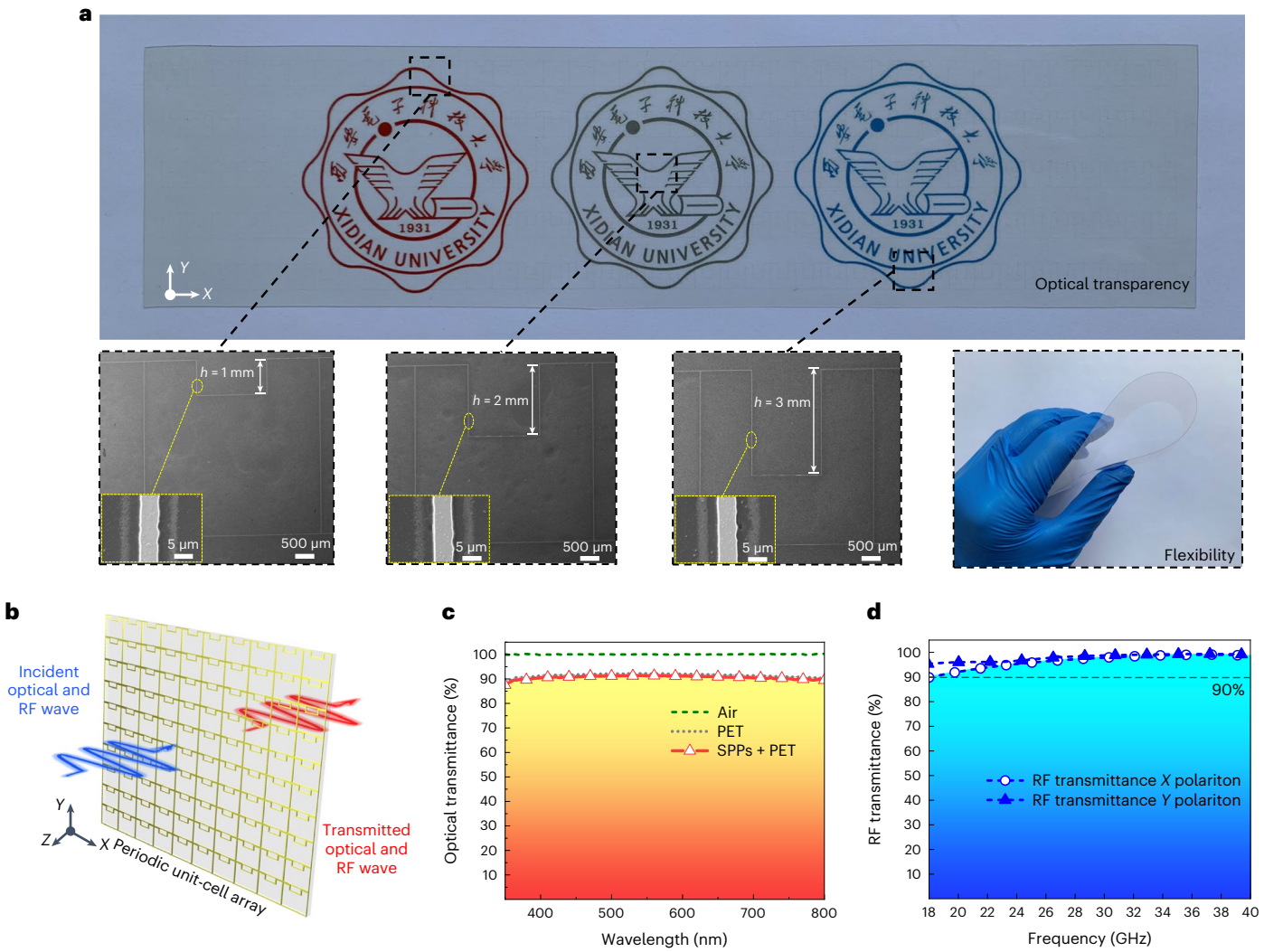


**Fig. 3 | Demonstrations of optical and radiofrequency transparency. a**, Photographs of the quasi-1D SPP structures corresponding to Fig. 1a, which demonstrate great flexibility and excellent optical transparency. **b**, Periodic quasi-1D SPP unit-cell array for strictly describing the transmittances. **c**, Experimental optical transmittance of the periodic SPP unit-cell array, which is above 90% over the visible spectrum. **d**, Experimental radiofrequency transmittance of the periodic SPP unit-cell array, which is above 90% over 18–40 GHz.

Figure 6 shows the experimental validation of the wireless communication scheme. Figure 6a shows the quasi-1D SPP-based/ITO-based data transfer system without a barrier. To visualize the attenuation of actual long-distance communication, the distance between the transmitter and the receiver is 2.5 m, and the quasi-1D SPP transceiver and ITO transceiver are adopted for comparison with the same transmitting power of −40 dBm. Figure 6b shows the quasi-1D SPP-based data transfer system with a quasi-1D SPP/ITO barrier. The distance between the transmitter and the receiver is set to 1 m to better shield the radiation wave and strictly evaluate the impact of radiofrequency transmittance on data transmission. Correspondingly, the transmitting power is adjusted to −48 dBm to satisfy Friis's transmission formula, and the quasi-1D SPP transceiver and ITO transceiver are adopted as the barrier for comparison.

Figure 6c shows comparison photographs of the fabricated quasi-1D SPP transceiver and ITO transceiver; the square resistance of ITO is 1 Ω/square, which is a common value in high-conductivity devices. The quasi-1D SPP transceiver has higher optical transmittance, and this method not only improves the optical transmittance, but also presents an invisible configuration. Figure 6d provides a comparison of image quality between the quasi-1D SPP-based and the ITO-based data transfer systems without the barrier.

The traditional method relying on ITO is subject to the materials' intrinsic properties. As a result, conductivity (carrier density) and optical transparency are mutually restricted, and even if ITO with high conductivity (1 Ω/square) is adopted the operation efficiency in the wireless communication systems will deteriorate (Supplementary Note 10). This leads to a sharp drop in signal strength and communication distance.

As verified in Fig. 6d, the quasi-1D SPP-based data transfer system shows excellent communication quality. In contrast, the image received by the ITO system is severely distorted. Figure 6e provides a comparison of image quality between quasi-1D SPP and ITO barriers. ITO is also unable to offer radiofrequency transparency, and ITO-based devices will block the communication of other devices, which is not conducive to the integration of communication systems. Our wireless communication system thus offers higher optical transmittance and communication quality than the traditional ITO approach. The high radiofrequency transmittance of our metadevice approach also benefits integrated communication and electromagnetic stealth.

https://doi.org/10.1038/s41928-023-00995-z

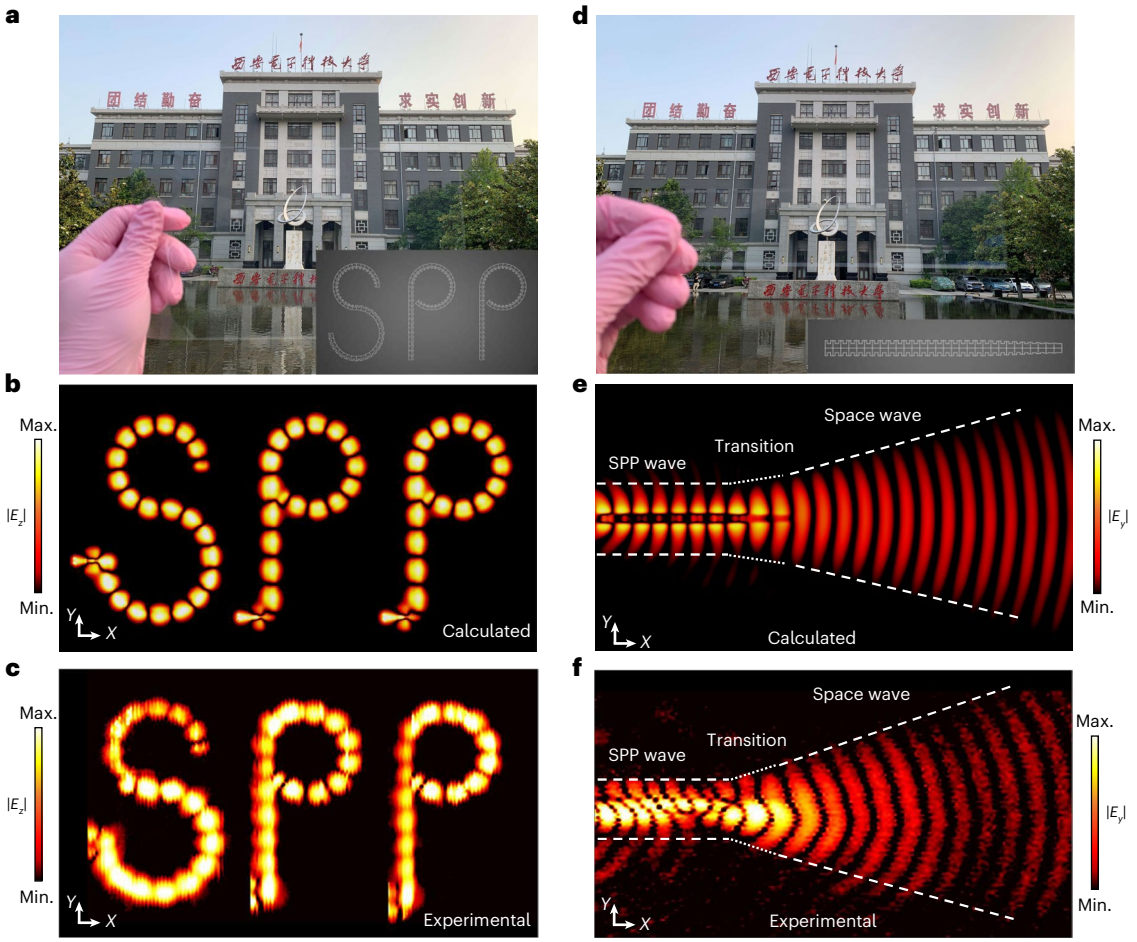


**Fig. 4 | Transparent quasi-1D SPP metadevices. a**, Photographs of the SPP-shaped quasi-1D SPP waveguides. **b**,**c**, Calculated and experimental electric field ($|E_z|$) distributions of the SPP-shaped quasi-1D SPP waveguides, showing excellent topological robustness. **d**, Photographs of the quasi-1D structured SPP wave to space wave converter. **e**,**f**, Calculated and experimental electric field ($|E_y|$) distributions of the SPP wave to space wave converter; the confined SPP wave effectively converts to a space wave.

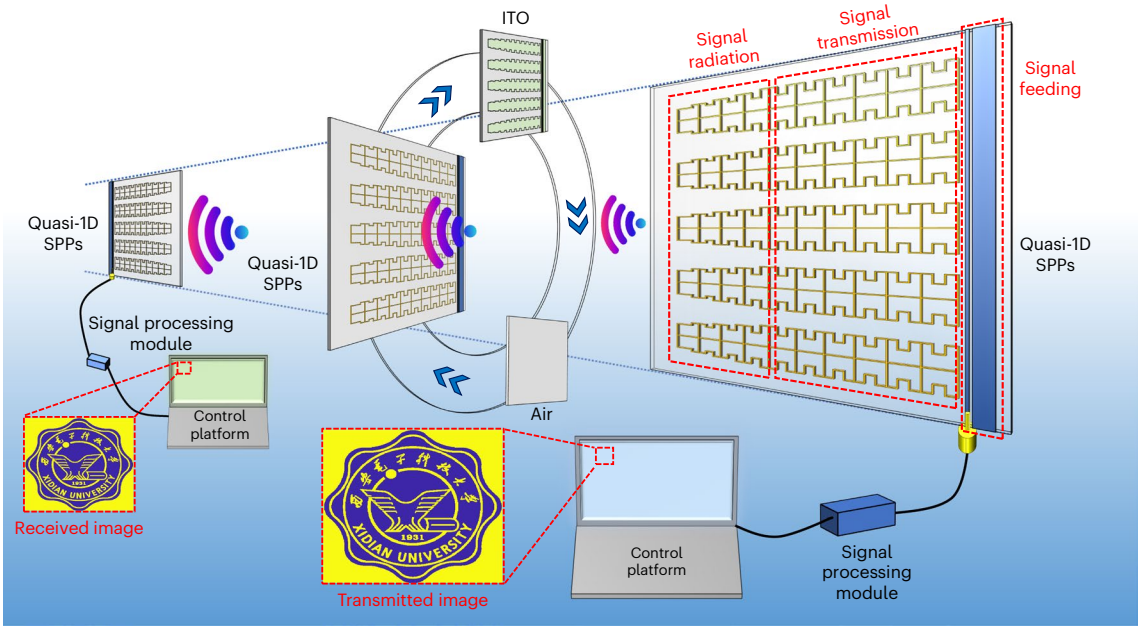


**Fig. 5 | Schematic of wireless communication scheme based on optically and radiofrequency-transparent metadevices.** In this scheme, a colour image is transmitted from the transmitter to the receiver with/without a barrier under a message transmission rate of 112.5 Kbps, and the traditional ITO-based approach is adopted for comparison.

https://doi.org/10.1038/s41928-023-00995-z

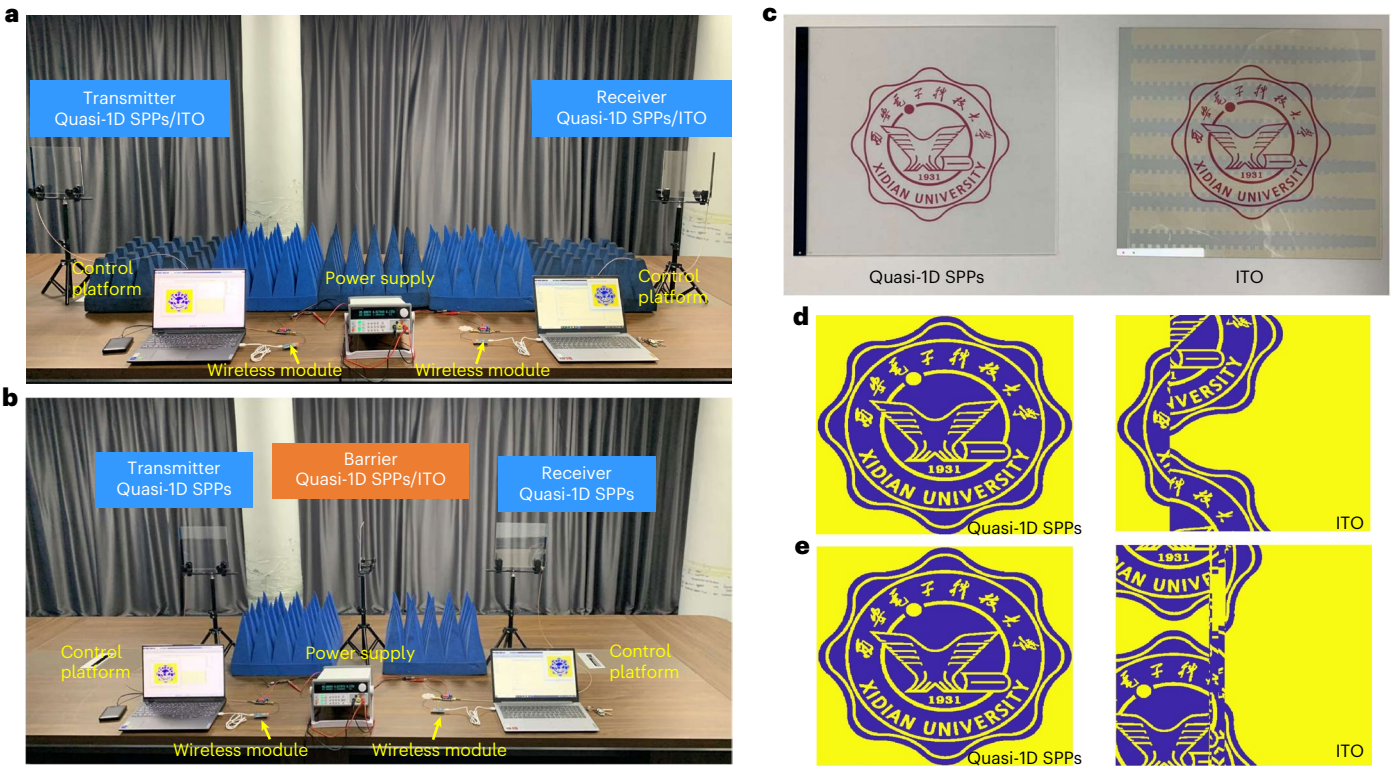


**Fig. 6 | Experimental validation of the wireless communication scheme based on optically and radiofrequency-transparent metadevices. a**, Quasi-1D SPP-based/ITO-based data transfer under the same transmitted power of −40 dBm, without a barrier. **b**, Quasi-1D SPP-based data transfer under the transmitted power of −48 dBm, with the quasi-1D SPP/ITO barrier. **c**, Comparison photographs of the quasi-1D SPP transceiver and the ITO transceiver. **d**, Comparison of image quality between quasi-1D SPP-based and ITO-based data transfer without the barrier. **e**, Comparison of image quality between quasi-1D SPP and ITO barriers in quasi-1D SPP-based data transfer.

## Conclusions

We have reported metadevices that are based on quasi-1D SPP structures and offer optical and radiofrequency transparency. We used the approach to create SPP-shaped waveguides with topological robustness and converters for turning SPP waves into space waves. We also used the quasi-1D SPP metadevices to create a wireless communication scheme for image transfer. Our technology provides an optically invisible configuration, radiofrequency transparency and high communication performance, and could be used to develop transparent metadevices for use in integrated communications, solar energy harvesting and electromagnetic stealth.

## Methods

### Calculations

Throughout this paper, the full-wave simulations (or numerical calculations) are performed using the commercial finite-integration technique software CST Microwave Studio. In dispersion analyses (Fig. 1e and Fig. 2b), the Eigenmode Solver is adopted, and the periodic boundary condition is imposed with a phase shift in the $X$ direction. In radiofrequency transparency calculations, the Frequency Domain Solver is adopted with periodic boundary conditions in both $X$ and $Y$ directions. The rest of the simulations and calculations are performed using the Time Domain Solver. All the in-plane field maps in the text are recorded at the plane 2 mm above the structures.

### Fabrications

The samples are fabricated by photolithography technology. First, a 1 μm copper layer is plated on the 100-μm-thick PET substrate by vacuum evaporation. After this, the copper layer is covered with photoresist by spin coating. Then, the photoresist is exposed to a pattern of intense light and the positive photoresist becomes soluble in the developer. As the next step, a liquid (wet) chemical agent removes the copper layer of the substrate in the areas that are not protected by the photoresist and the designed pattern is achieved. Finally, the photoresist is removed from the substrate, and the fabricated samples are cleaned and heated without leaving any residue.

### Measurements

For mode distribution (electric field) measurement (Fig. 4c,f), the near-field scanning system is utilized to map the localized electric field in the plane 2 mm above the SPP structures. The experimental set-up consists of an Agilent E5071C vector network analyser, two stepping motors for 2D scanning and a monopole antenna as a detector. The detector, controlled by two computer-controlled stepping motors, is fixed at 2 mm above the samples and moved to scan the electric field distributions with the scanning step of 1 mm (Supplementary Note 6). The data of electric field magnitude are collected and recorded by the network analyser. To ensure the accuracy of the experiment, the whole experiment is carried out in an anechoic chamber. The optical transmittance (Fig. 3c) is measured using a Hitachi UH4150 spectrometer. For radiofrequency transparency measurement (Fig. 3d), the experimental set-up consists of an Anritsu MS4632A vector network analyser, a bracket, a reflective plate for shielding noise wave and two horn antennas for transmitting and receiving. The distance between the reflective plate and the two horn antennas is 0.6 m, which ensures that the radiofrequency wave is almost a plane wave when it reaches the sample (Supplementary Note 8). There is a 10 cm × 10 cm square hole in the reflective plate. The radiofrequency wave will be transmitted by horn antenna 1 and received by horn antenna 2 through the square

hole. The sample was placed in the square hole of the reflective plate for measurement of the radiofrequency transmittance. For wireless communication, a colour image is transmitted from the transmitter to the receiver under a message transmission rate of 112.5 Kbps with a carrier frequency of 5.8 GHz: the computer digitizes the image, the signal processing module converts the data into the radiofrequency signal and then the radiofrequency signal is fed into the transceiver.

## Data availability

The data that support the findings of this study are available from the corresponding authors upon reasonable request.

## References


1. Fan, R. H. et al. Transparent metals for ultrabroadband electromagnetic waves. *Adv. Mater.* **24**, 1980–1986 (2012).
2. Luo, J. et al. Ultratransparent media and transformation optics with shifted spatial dispersions. *Phys. Rev. Lett.* **117**, 223901 (2016).
3. Palmer, S. J. et al. Extraordinarily transparent compact metallic metamaterials. *Nat. Commun.* **10**, 2118 (2019).
4. Chu, H. et al. Diffuse reflection and reciprocity-protected transmission via a random-flip metasurface. *Sci. Adv.* **7**, eabj0935 (2021).
5. Chu, H. et al. Invisible surfaces enabled by the coalescence of anti-reflection and wavefront controllability in ultrathin metasurfaces. *Nat. Commun.* **12**, 4523 (2021).
6. Zhang, L. et al. Correlated metals as transparent conductors. *Nat. Mater.* **15**, 204–210 (2016).
7. Li, S. et al. Nanometre-thin indium tin oxide for advanced high-performance electronics. *Nat. Mater.* **18**, 1091–1097 (2019).
8. Datta, R. S. et al. Flexible two-dimensional indium tin oxide fabricated using a liquid metal printing technique. *Nat. Electron.* **3**, 51–58 (2020).
9. Sim, K. et al. Three-dimensional curvy electronics created using conformal additive stamp printing. *Nat. Electron.* **2**, 471–479 (2019).
10. Park, S.-I. et al. Printed assemblies of inorganic light-emitting diodes for deformable and semitransparent displays. *Science* **325**, 977–981 (2009).
11. Hong, S. et al. Transparent and flexible antenna for wearable glasses applications. *IEEE Trans. Antennas Propag.* **64**, 2797–2804 (2016).
12. Potti, D. et al. A novel optically transparent UWB antenna for automotive MIMO communications. *IEEE Trans. Antennas Propag.* **69**, 3821–3828 (2021).
13. Barnes, W. L., Dereux, A. & Ebbesen, T. W. Surface plasmon subwavelength optics. *Nature* **424**, 824–830 (2003).
14. Fang, N., Lee, H., Sun, C. & Zhang, X. Sub-diffraction-limited optical imaging with a silver superlens. *Science* **308**, 534–537 (2005).
15. Ozbay, E. Plasmonics: merging photonics and electronics at nanoscale dimensions. *Science* **311**, 189–193 (2006).
16. Kawata, S., Inouye, Y. & Verma, P. Plasmonics for near-field nano-imaging and superlensing. *Nat. Photon.* **3**, 388–394 (2009).
17. Gramotnev, D. K. & Bozhevolnyi, S. I. Plasmonics beyond the diffraction limit. *Nat. Photon.* **4**, 83–91 (2010).
18. Pendry, J. B., Martin-Moreno, L. & Garcia-Vidal, F. J. Mimicking surface plasmons with structured surfaces. *Science* **305**, 847–848 (2004).
19. García de Abajo, F. J. & Sáenz, J. J. Electromagnetic surface modes in structured perfect-conductor surfaces. *Phys. Rev. Lett.* **95**, 233901 (2005).
20. Gao, F. et al. Probing topological protection using a designer surface plasmon structure. *Nat. Commun.* **7**, 11619 (2016).
21. Gong, S. et al. Transformation of surface plasmon polaritons to radiation in graphene in terahertz regime. *Appl. Phys. Lett.* **106**, 223107 (2015).
22. Zhang, H. C. et al. A plasmonic route for the integrated wireless communication of subdiffraction-limited signals. *Light Sci. Appl.* **9**, 113 (2020).
23. Xue, T. et al. Ultrasensitive detection of miRNA with an antimonene-based surface plasmon resonance sensor. *Nat. Commun.* **10**, 28 (2019).
24. Balaur, E. et al. Plasmon-induced enhancement of ptychographic phase microscopy via sub-surface nanoaperture arrays. *Nat. Photon.* **15**, 222–229 (2021).
25. Ozaki, M., Kato, J.-I. & Kawata, S. Surface-plasmon holography with white-light illumination. *Science* **332**, 218–220 (2011).
26. Freire-Fernández, F. et al. Magnetic on–off switching of a plasmonic laser. *Nat. Photon.* **16**, 27–32 (2022).
27. Yu, N. et al. Designer spoof surface plasmon structures collimate terahertz laser beams. *Nat. Mater.* **9**, 730–735 (2010).
28. Zhang, H. C., Cui, T. J., Zhang, Q., Fan, Y. & Fu, X. Breaking the challenge of signal integrity using time-domain spoof surface plasmon polaritons. *ACS Photon.* **2**, 1333–1340 (2015).
29. Guan, D. F., You, P., Zhang, Q. F., Xiao, K. & Yong, S. W. Hybrid spoof surface plasmon polariton and substrate integrated waveguide transmission line and its application in filter. *IEEE Trans. Microw. Theory Tech.* **65**, 4925–4932 (2017).
30. Haffner, C. et al. Low-loss plasmon-assisted electro-optic modulator. *Nature* **556**, 483–486 (2018).
31. Dong, J. et al. Versatile metal-wire waveguides for broadband terahertz signal processing and multiplexing. *Nat. Commun.* **13**, 741 (2022).
32. Shen, X., Cui, T. J., Martin-Cano, D. & Garcia-Vidal, F. J. Conformal surface plasmons propagating on ultrathin and flexible films. *Proc. Natl Acad. Sci. USA* **110**, 40–45 (2013).
33. Chen, L. et al. Mode splitting transmission effect of surface wave excitation through a metal hole array. *Light Sci. Appl.* **2**, e60 (2013).
34. Fusella, M. A. et al. Plasmonic enhancement of stability and brightness in organic light-emitting devices. *Nature* **585**, 379–382 (2020).
35. Liu, X. et al. Microcavity electrodynamics of hybrid surface plasmon polariton modes in high-quality multilayer trench gratings. *Light Sci. Appl.* **7**, 14 (2018).
36. Larkin, I. A. et al. Superanomalous skin effect for surface plasmon polaritons. *Phys. Rev. Lett.* **119**, 176801 (2017).
37. Maniyara, R. A. et al. Tunable plasmons in ultrathin metal films. *Nat. Photon.* **13**, 328–333 (2019).
38. Tang, W. X., Zhang, H. C., Ma, H. F., Jiang, W. X. & Cui, T. J. Concept, theory, design, and applications of spoof surface plasmon polaritons at microwave frequencies. *Adv. Opt. Mater.* **7**, 1800421 (2019).
39. Kang, S. H. & Jung, C. W. Transparent patch antenna using metal mesh. *IEEE Trans. Antennas Propag.* **66**, 2095–2100 (2018).


## Acknowledgements

B.W. is grateful for financial support by the National Natural Science Foundation of China (NSFC) under grants 62171348, 62071357 and U19A2055. W.-X.T. is grateful for financial support by the National Natural Science Foundation of China (grant 61971134). T.-J.C. is grateful for financial support by the National Natural Science Foundation of China (grant 62288101). H.-R.Z. and B.W. acknowledge Y. Hao at the Queen Mary University of London for substantial support and assistance on mechanism analysis and representation.

## Author contributions

H.-R.Z. and B.W. conceived the idea and designed the experiment. B.W. and T.-J.C. supervised the project. H.-R.Z., B.C. and W.-H.L. performed the experiments. H.-R.Z. and B.C. analysed the experimental data. H.-R.Z. performed the simulation. H.-R.Z. and B.W. wrote the initial manuscript. B.C. upgraded the illustration presentation. W.-X.T., T.-J.C. and D.-P.H. revised and improved the manuscript. All the authors discussed the results and commented on the manuscript.

## Competing interests

The authors declare no competing interests.

## Additional information

**Supplementary information** The online version contains supplementary material available at https://doi.org/10.1038/s41928-023-00995-z.

**Correspondence and requests for materials** should be addressed to Bian Wu or Tie-Jun Cui.

**Peer review information** *Nature Electronics* thanks Yun Lai and the other, anonymous, reviewer(s) for their contribution to the peer review of this work.